Effects of soil surface degradation and vehicle momentum on dust emissions and visibility reduction from unpaved roads

Mickael Le Vern, Andry Razakamanantsoa, Frédéric Murzyn, Frédérique Larrarte, Véronique Cerezo

Author accepted manuscript published in : Transportation Geotechnics 37(2022). Elsevier
https://doi.org/10.1016/j.trgeo.2022.100842

Effects of soil surface degradation and vehicle momentum on dust emissions and visibility reduction from unpaved roads

Mickael Le Vern[1*], Andry Razakamanantsoa[1], Frédéric Murzyn[2], Frédérique Larrarte[3], Véronique Cerezo[4]

[1] University Gustave Eiffel, GERS-GIE, Allée des Ponts et Chaussées, 44344, Bouguenais, France

[2] ESTACA West Campus, Department of Mechanical Engineering, Rue Georges Charpak, 53000, Laval, France

[3] University Gustave Eiffel, GERS-SRO, Boulevard Newton, 77447, Champs sur Marne, France

[4] University Gustave Eiffel, AME-EASE, 25 Avenue François Mitterrand, 69675, Bron, France

*Corresponding author: mickael.le-vern@ec-nantes.fr

Abstract

Unpaved roads are built on the basis of soil compaction. Therefore, the operation of vehicles on these roads results in dust emissions. As the number of passing vehicles increases, the soil surface gradually degrades under shearing caused by the tires. This enhances emissions and reduces visibility, increasing health and environmental related issues as well as the risk of collisions.

The present study was conducted to quantify the effect of surface degradation on dust emissions from several types of vehicles travelling on different soils and assess the evolution of security risks in the vicinity of unpaved roads.

Three types of vehicles (a passenger car, a 4WD vehicle and a truck) have been run on an experimental road covered by four different types of soil particles. Each test consisted in driving one of the vehicles at a given speed (30, 45 or 60 $km.h^{-1}$) on one of the types of particles previously spread on the road at a given mass per unit area (200, 400 or 600 $g.m^{-2}$). The mass concentration of resuspended particles was measured from the roadside using an Optical Particle Counter (OPC) while the visibility reduction was simultaneously recorded at the same location. The results show that PM_{10} emission factors increase linearly with vehicle momentum for vehicles without mud flaps. The presence of such appendices can reduce dust emissions by a factor of 7. Moreover, although not considered in conventional models, the state of degradation of unpaved roads may be a key factor regarding dust emissions. The study has also shown that soils with similar silt content can result in very different emission factors. An emission model has then been developed, based on the clay content of the particles. Indeed, this geotechnical parameter is more relevant to characterize the fine soil propensity to generate dust. PM_{10} emissions are correlated with the reduction of visibility according to a power law for the truck tests.

An interesting finding of this work is the fact that the present results can be extended to earthwork sites where visibility problems require spraying of water on the traffic lanes. Improving the modeling of the mechanisms generating dust lift and the associated safety risks is indeed essential for a more efficient use of water on construction sites.

Keywords: Dust re-suspension, Vehicle traffic, Unpaved road, Surface degradation, Test track, Visibility

Nomenclature

c	clay content of the particles	(%)
C	PM_{10} mass concentration corrected	($\mu g.m^{-3}$)
$C_{measured}$	PM_{10} mass concentration measured by the optical particle counter	($\mu g.m^{-3}$)
d_p	Particle diameter	(m)
D	Soil surface degradation	($kg.m^{-2}$)
$EF_{industrial}$	Mass of PM_{10} per vehicle kilometer travelled (vkt) on industrial unpaved roads	($g.vkt^{-1}$)
EF_{model}	Model developed in this study for mass of PM_{10} per vehicle kilometer travelled	($g.vkt^{-1}$)
EF_{public}	Mass of PM_{10} per vehicle kilometer travelled (vkt) on public unpaved roads	($g.vkt^{-1}$)

L_c	Characteristic length	(m)
M	Moisture content of the particles	(%)
M_{om}	Vehicle momentum ($S \times W$)	(kg.m.s^{-1})
N	Number of PM_{10} mass concentration values measured	(-)
$\overline{PM_{10}}$	Mean PM_{10} mass concentration	(µg.m^{-3})
s	Silt content of the soil (% of particles with $d_p < 75\mu m$)	(%)
S	Vehicle speed	(m.s^{-1})
S_{tk}	Stokes number of the particle ($\frac{1}{18}\frac{\rho_p d_p U_0}{\mu L_c}$)	(-)
U	Sampling velocity	(m.s^{-1})
U_0	Wind velocity	(m.s^{-1})
V	Visibility	(km)
W	Vehicle weight	(kg)
Δt	Duration over which the dust plume impacts the optical particle counter	(s)
Δz	Dust plume vertical interval	(m)
η_{asp}	Aspiration efficiency of the optical particle counter	(%)
η_{sample}	Sampling efficiency of the optical particle counter	(%)
η_{trans}	Transport efficiency in the nozzle of the optical particle counter	(%)
θ	Angle between the wind and sampling directions	(°)
μ	Dynamic air viscosity	(kg.m^{-1}.s^{-1})
ρ_p	Particle density	(kg.m^{-3})

1. Introduction

The control of dust generated by human activities is a major objective for air quality improvement. The degradation of soils is a key factor for the resuspension of particles in the atmosphere. In particular, the traffic of vehicles on unpaved roads is a major source of dust emissions (Thenoux et al., 2007; Flores-Márgez et al., 2014). Unpaved roads are built on the basis of soil compaction without surface coating. Where contact between the soil and the vehicle wheels is made, the aggregates of soil particles can be torn off and then crumbled (Le Vern et al., 2020a). This leads to the formation of fine particles on the road surface, which can be lifted by shear stresses and turbulent aerodynamic processes induced by the passing vehicles (Etyemezian et al., 2003; Williams et al., 2008; Gérardin and Midoux, 2015; Le Vern et al., 2020b). Important amounts of dust are emitted through such mechanisms. Unpaved roads, for instance, are responsible for 30% to 50% of the PM_{10} (particles having an aerodynamic diameter below 10µm) emissions in southern United States and northern Mexico (Kuhns et al., 2005). Studies often focus on PM_{10} because it dominates the mass distribution of dust emitted by vehicles on sandy and silty soils (Pinnick et al., 1985).

Airborne dust particles cause environmental and public health related problems (Vardaka et al., 1995; Pope and Dockery, 2006). They are also responsible for reduced visibility (Baddock et al., 2014) associated with significant collision risks in the areas of vehicle traffic (Lankarani et al., 2014; Ashley et al., 2015; Bhattachan et al., 2019). This concern is particularly important on earthmoving sites and quarries where the activities are highly dusty (Muleski et al., 2005; Faber et al., 2015; Noh et al., 2018). It is worth noting that dust emission is ranked as the second most common risk for many professionals of the construction sector (Serpell et al., 2013). Visibility reduction is often assessed through visual criteria, which lead to the spraying of water on the traffic lanes of the construction sites (USEPA, 1988). It should be noted, moreover, that no documents are currently available as guides on how much water should be used to reduce dust emission or on how the time interval between two sprayings could be accurately defined (NIOSH, 2012). For a better management of water, it is essential to quantify the evolution of the dust emissions induced by the vehicles on the road.

The most widely used model for estimating PM_{10} emissions from vehicles on unpaved roads to date is "AP-42: Compilation of Air Emissions Factors" developed by the US Environmental Protection Agency (USEPA, 2006). For the vehicles operating on unpaved surfaces of industrial sites like mines and quarries, the emission factor *EF* estimation is given by Eq. (1):

$$EF_{industrial} = 422.85 \times \left(\frac{s}{12}\right)^{0.9} \times \left(\frac{W}{3000}\right)^{0.45} \quad (1)$$

and, for publicly accessible unpaved roads, Eq. (2) is used:

$$EF_{public} = 507.42 \times \frac{\left(\frac{s}{12}\right) \times \left(\frac{S}{13.4}\right)^{0.5}}{\left(\frac{M}{0.5}\right)^{0.2}} \quad (2)$$

where *EF* is the PM_{10} emission factor (mass of PM_{10} in grams emitted per vehicle kilometer travelled, i.e., $gPM_{10}.vkt^{-1}$), *s* is the surface material silt content (% of particles smaller than 75 µm), *W* is the mean vehicle weight (kg), *S* is the mean vehicle speed ($m.s^{-1}$) and *M* is the surface material moisture content (%).

In these models, the PM_{10} emission factor is considered constant regardless of the number of passing vehicles. They do not take into account the evolving mechanisms of soil degradation, in particular tearing off and crumbling of particle aggregates by tires (Le Vern et al., 2020a). Moreover, the surfaces on which the vehicles travel are only roughly described through the sole criterion of the silt content. These two purely empirical USEPA models (Eq. (1) and (2)) can be applied to the sites used to develop them but are difficult to generalize. Indeed, when comparing these models with field measurements, some significant differences are observed, up to several orders of magnitude (Gillies et al., 2005; Muleski et al., 2005, Kuhns et al., 2010). It is therefore essential to examine the dust emission mechanisms in greater depth in order to improve the robustness of estimation models.

The objective of this research is first to examine the effects of unpaved road surface degradation on dust emissions. Therefore, tests are conducted in which the degradation is characterized through the dust loading on the road surface, i.e., the mass of torn-off particles per unit area. Different quantities of particles are spread on the test track before the vehicle is run on it. Various types of particles are considered in order to discuss the relevance of the "silt content" parameter in emission models. The effect of vehicle momentum on dust emissions is assessed by driving three different types of vehicles (a light passenger car, a 4WD vehicle equipped with mud flaps and a heavy truck) over the spread particles at different speeds. Dust emissions on the side of the road are considered for this work. A companion paper (Le Vern et al., 2021) examines the dust emissions in the wake of the vehicle tires.

The second purpose of this study is to investigate the safety risks caused by vehicle-induced dust plumes. Using the measurements of the roadside concentrations of particulate matter and the corresponding visibility reduction at the same location, a model is established linking visibility and suspended dust. The discussion is conducted with a view to optimizing risk management by spraying water on the traffic lanes of the construction sites.

The methodology is presented in the second part of the paper, including a description of the vehicles, the test tracks, the particles, the experimental procedure and data processing. Then, the results are detailed and discussed. The last section is dedicated to conclusions and future research works.

2. Materials and methods

2.1 Vehicles used and test tracks

Three different vehicles are used for the tests: a Renault Clio III, a 4WD Ford Ranger and a Volvo FMX 450 truck. The Renault Clio ranks among the best-selling cars in Europe and is representative of small passenger cars. The 4WD vehicle is twice the mass of the Clio and has larger dimensions. Moreover, this car is more likely to be used on unpaved roads and earthwork lanes. The Volvo FMX 450 is one of the largest trucks in its class (cab-over semi-trailers) for construction and earthmoving works. Prior to testing, the truck's dump box has been filled with material an then used at its maximum gross weight (approximately 32 tons). This configuration reflects the most severe conditions of heavy-duty vehicle traffic that can generate dust emissions. The three test vehicles are displayed in Figure 1. Their characteristics are detailed in Table 1. The tread pattern of the tires consists of longitudinal ribs for the Clio and the 4WD vehicle and of block treads for the truck.

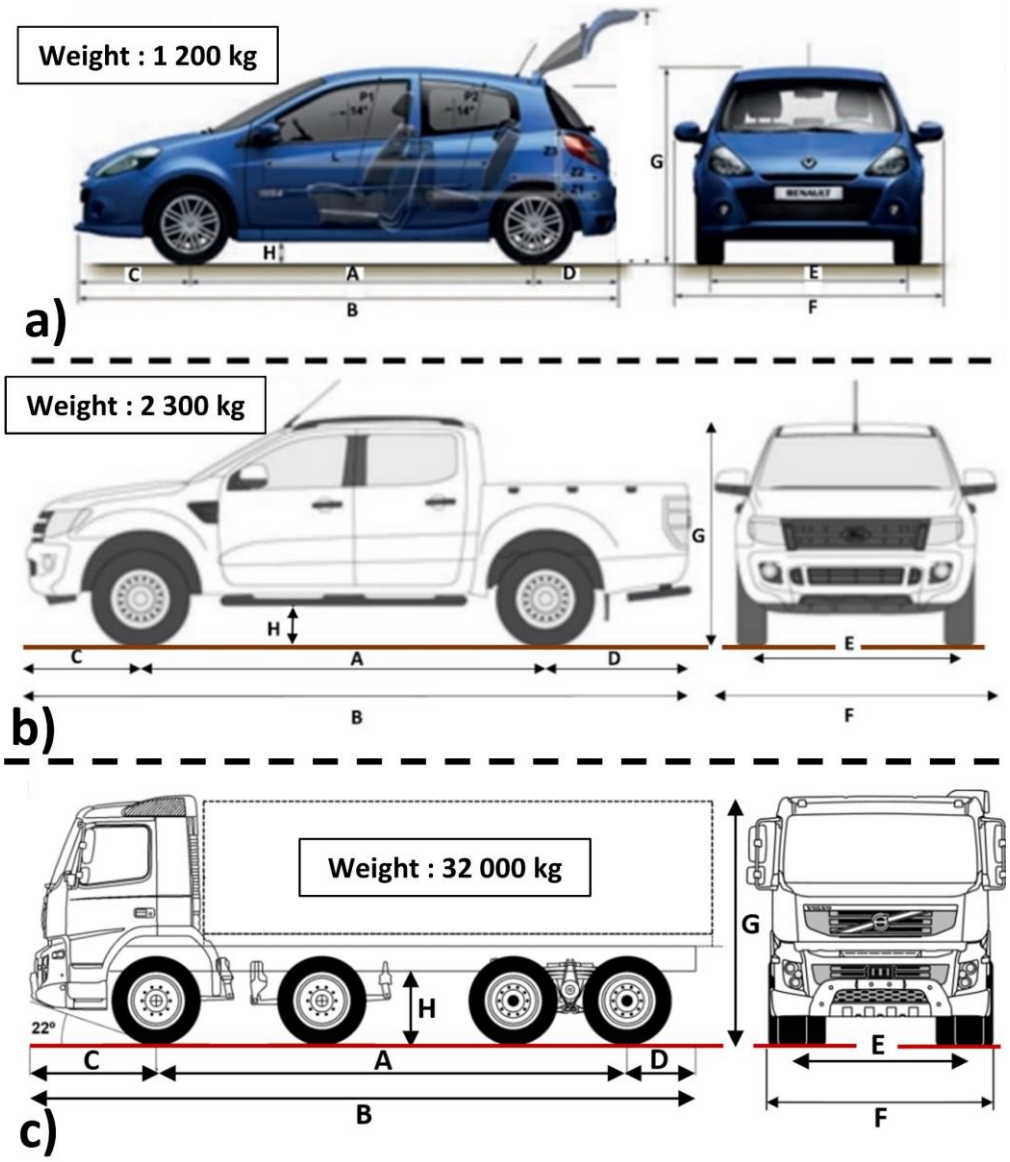

Figure 1: Front and side view of the vehicles: a) Renault Clio III; b) 4WD Ford Ranger and c) Volvo FMX truck

Table 1 : Characteristics of the vehicles

Characteristic (letter corresponds to Figure 1)	**Vehicle**		
	Renault Clio III	**4WD Ford Ranger**	**Truck Volvo FMX**
A: Wheelbase (mm)	2,575	3,220	5,970
B: Overall length (mm)	4,027	5,350	8,665
C: Front overhang (mm)	830	908	1,520
D: Rear overhang (mm)	622	1,226	1,175
E: Front/rear tire spacing (mm)	1,470	1,560	2,180
F: Width with mirrors (mm)	2,025	2,163	2,495
G: Empty height (mm)	1,493	1,820	3,122
H: Ground clearance (mm)	120	229	924
Wheel diameter (mm)	610	780	1,090
Weight (kg)	1,200	2,300	32,000

The tests are carried out on two asphalt test tracks (Figure 2). The tests involving the Renault Clio III and the Ford Ranger were conducted during summer 2019 on test track #1 (Figures 2-a and 2-b), whereas those involving the Volvo truck were conducted in September 2020 on test track #2 (Figure 2-c). For both measurement campaigns, the surface roughness of the two tracks is the same for comparative purposes. For confirmation of similarity, six measurements distributed along the running zone of each track using a portable ELATextur rotary profilometer have been carried out. The mean surface roughness Ra, defined as the arithmetical mean deviation of the assessed profile (Whitehouse, 2012), was 662 µm for track #1 and 689 µm for track #2, respectively. These values are very close (a 4% difference). Consequently, the experimental conditions can be considered similar regarding surface roughness.

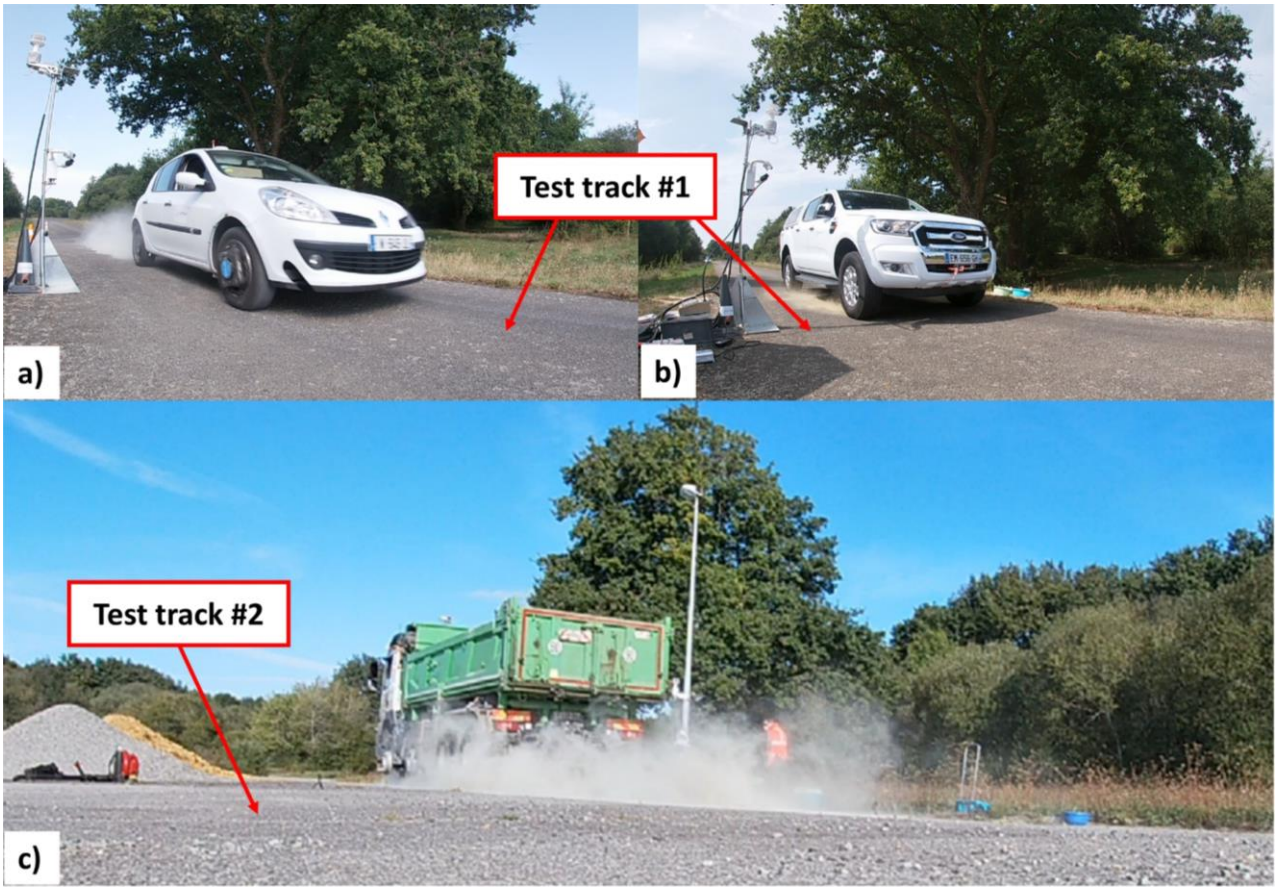

Figure 2: Experimental test tracks in University Gustave Eiffel (Bouguenais, France) used for the tests with the Renault Clio III and the 4WD Ford Ranger (a and b) and with the Volvo FMX truck (c)

2.2 Characteristics of the particles

Four different types of particles are used for the tests: a clay mixture composed of montmorillonite and illite (cosmetic green clay CATTIER, denoted as "GC") and three silty soils sampled from various earthwork sites in Europe (Val d'Europe (SVE) and Strasbourg (SS) in France, Marche les Dames (SMD) in Belgium). The last three types of soils are the most common soils found on construction sites. They have similar silt contents (between 95% and 100%) but differ in their other geotechnical properties like clay content or liquid limit (Figure 3 and Table 2). Because silt content is the parameter used to quantify dust emission in the reference models (Eq. (1) and (2)), the tests are carried out to verify whether this criterion is sufficient to characterize particle lift or if other geotechnical parameters must be considered. In Table 2, the Liquid Limit and Plastic Limit are parameters used to quantify the behavior of the soil when it is moistened. They were measured in accordance with the ISO 17892-12:2018 standard (ISO, 2018). Combined with the granulometric properties (passing at 2 µm and 75 µm), they can be used for classification of the particles. The corresponding classification is presented in Table 2 according to the American Society for Testing Material standard (ASTM, 2017) and the French Guide for road earthworks (GTR, 2000). The Methylene Blue Value of the soils (ASTM, 2019), which is an indirect measure of the specific surface of the finest particles, is also presented.

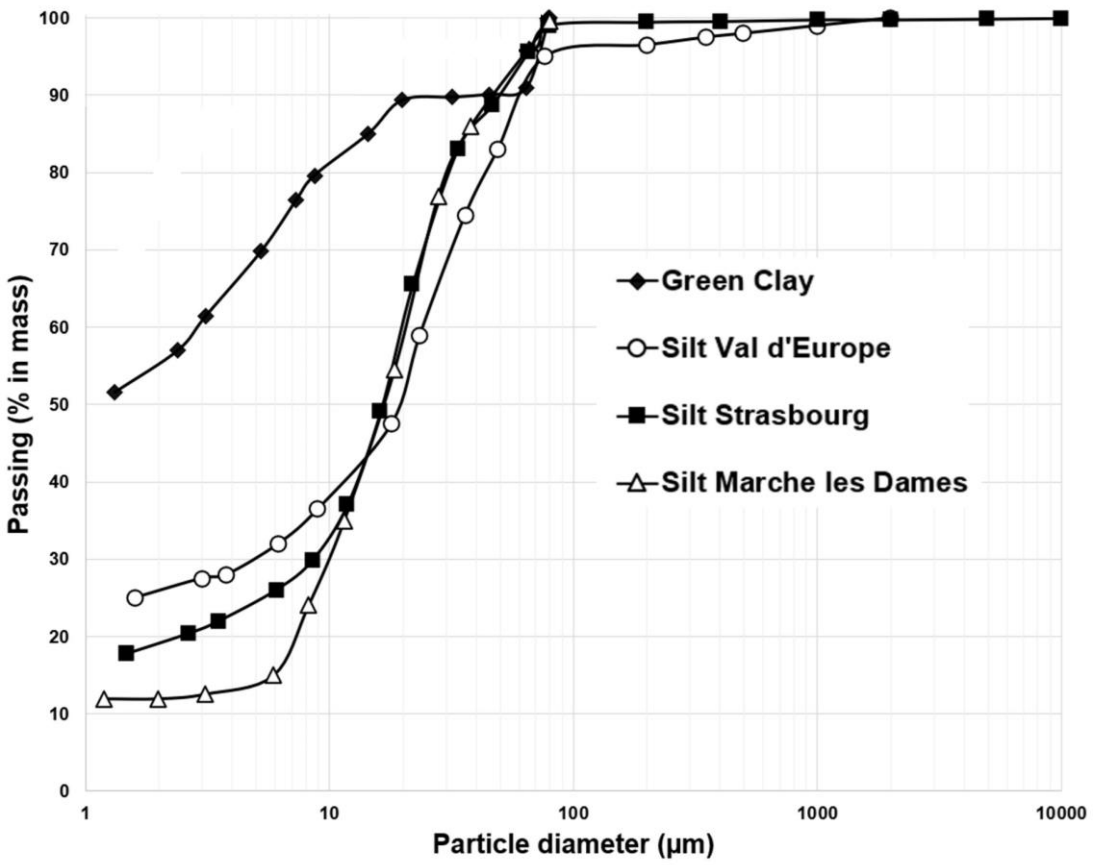

Figure 3: Particles size distributions of the soils

Table 2: Geotechnical properties of the soil particles

Particles (denotation)	**% < 2 µm**	**% < 75 µm**	**Liquid Limit (%)**	**Plastic Index (%)**	**Bulk density (kN/m^3)**	**Methylene Blue Value (g/100g)**	**Classification ASTM***	**Classification GTR****
Green Clay (GC)	53.0	100.0	50.7	15.7	26.9	5.6	MH: Elastic Silt	A2: Low plasticity Clay
Silt Val d'Europe (SVE)	26.0	95.0	36.5	15.7	25.4	3.9	CL: Lean Clay	A2: Silt
Silt Strasbourg (SS)	19.0	99.0	40.3	24.9	25.8	3.0	CL: Lean Clay	A2: Silt
Silt Marche les Dames (SMD)	12.0	99.5	31.0	11.0	25.9	2.5	CL: Lean Clay	A1: Loess

*American Society for Testing Material

** Guide des Terrassements Routiers (French guide for road earthworks)

2.3 Experimental methodology

In order to ensure complete removal of moisture from the particles used for testing, they are first dried in an oven at 105°C during 24 hours (ISO, 2014). Then, they are sieved through a 2-mm sieve to grind aggregates and finally packed in plastic bags. Before testing, the particles are spread homogeneously on the tracks using a fertilizer spreader. They are divided over two lines separated from each other by the distance corresponding to the spacing between the tires of the vehicle (1.47 m for the Clio, 1.56 m for the 4WD vehicle and 2.18 m for the truck, respectively). Each line is 3 m in length and 0.3 m in width for the tests with the Clio and the 4WD vehicle and 6 m in length and 0.54 in width for the truck. The widths of the lines are voluntarily larger than the widths of the tires (0.20 m for the Clio, 0.25 m for the 4WD vehicle and 0.315 m for the truck). For practical reasons, the lengths of the lines are defined according to the quantities of particles available and the length of the test vehicles. They are long enough to generate a dust plume on the side of the road, which is easily measurable and representative of the vehicle actual emissions. Three different quantities of particles per unit area are considered (200, 400 and 600 $g.m^{-2}$). They correspond to three distinct states of soil degradation: low, medium and high. These states of degradation have been determined in a previous study by running a wheel on different testing soils in a traffic simulator (Le Vern et al., 2020a). A mobile weather station is positioned on the side of the track to record temperature, relative humidity and wind speed and direction. The tests on test track #1 (test track #2) are conducted after 9 days (3 days) with no rainfall, under relative humidity conditions ranging between 50 and 80% (65 and 85 %), temperature conditions within the range 17-25°C (11-17 °C) and wind speed conditions from 0.5 to 2.4 $m.s^{-1}$ (0.7 to 2.6 $m.s^{-1}$). The prevailing wind directions were northwest on test track #1 and southwest on test track #2. Figure 4 presents the diagram of the experimental setup.

Each test consists in running successively one of the three vehicles at a prescribed speed (30, 45 or 60 $km.h^{-1}$) over one type of particles previously spread on the track at a given mass per unit area (200, 400 or 600 $g.m^{-2}$). The speed of 30 km/h corresponds to the traffic conditions imposed when the risk of dust resuspension is high (especially on construction sites). The speed of 45 km/h is often observed in cities or on construction sites. Testing at 60 km/h makes it possible to study what happens when the speed doubles compared with the initial 30 km/h and thus to highlight the impact of vehicle momentum on dust emission. For practical reasons, the tests with the truck have been conducted at 30 and 45 km/h only and the 4WD vehicle at 60 km/h only. The tests with the Renault Clio III, on the other hand, have been carried out at the three testing speeds. The three particle masses per unit area on the ground are tested with each vehicle. For reasons of stock availability, only the SVE soil is used for the tests with the Renault Clio III and the 4WD Ford Ranger.

The test tracks are made of asphalt concrete to ensure that only the particles that have been spread on the track can be raised by the test vehicle. This parameter could not have been controlled if the tests had been run on an unpaved road. Because asphalt pavements do not have the same roughness and are stiffer than unpaved roads, which are made of compacted soils, the tests here are not fully representative of the unpaved roads conditions. Indeed, on actual unpaved roads, tire tread and weight can remove and suspend particles from a certain depth below the soil surface, especially if the road presents surface imperfections (ruts, potholes, …). Soil degradation by tires has already been studied and discussed in a previous study (Le Vern et al., 2020a). The present study is the second step and was conducted to examine the effects of the state of degradation of the road on dust emissions. This experimental configuration makes it possible to extend the results to the problem of particle emissions due to the contamination of asphalt mixes. However, this contamination generally generates smaller quantities of particles than those studied here (Hussein et al., 2008; Hichri et al., 2019).

During the tests, an Optical Particle Counter (OPC) continuously measures the mass concentration of the suspended dust by suction from the side of the road at a data rate of 1 Hertz. The measurement station is placed on the side of the road in the direction of the prevailing wind, as shown in Figures 4-a and 4-b. Dust concentrations are measured at the height of 1.5 m from the ground. Preliminary tests have been carried out to determine the maximum concentration height by varying the measurement height between 1 m and 1.7 m. The maximum dust concentration is obtained at a height of 1.5 m, which is approximately the height of the dust plume centerline. The sensor is a PALAS Fidas Mobile dust analyzer equipped with a pump that sucks the particles contained in the ambient air. The particles then flow through a beam of LED light, which is subsequently scattered. A photomultiplier measures the angle of the scattered light. According to Mie's scattering theory (Mie, 1908), this angle depends on the size of the particle. Combined with a counting algorithm, the mass concentration of particles per unit volume ($\mu g/m^3$) can be estimated. The device provides particle size distribution over 71 sizes ranging between 0.17 and 26 µm (factory settings). The measurement range of the PM mass concentration is from 1 to 50 000 $\mu g.m^{-3}$. The apparatus has been previously calibrated using "MonoDust 1500", a calibration dust recommended by the manufacturer.

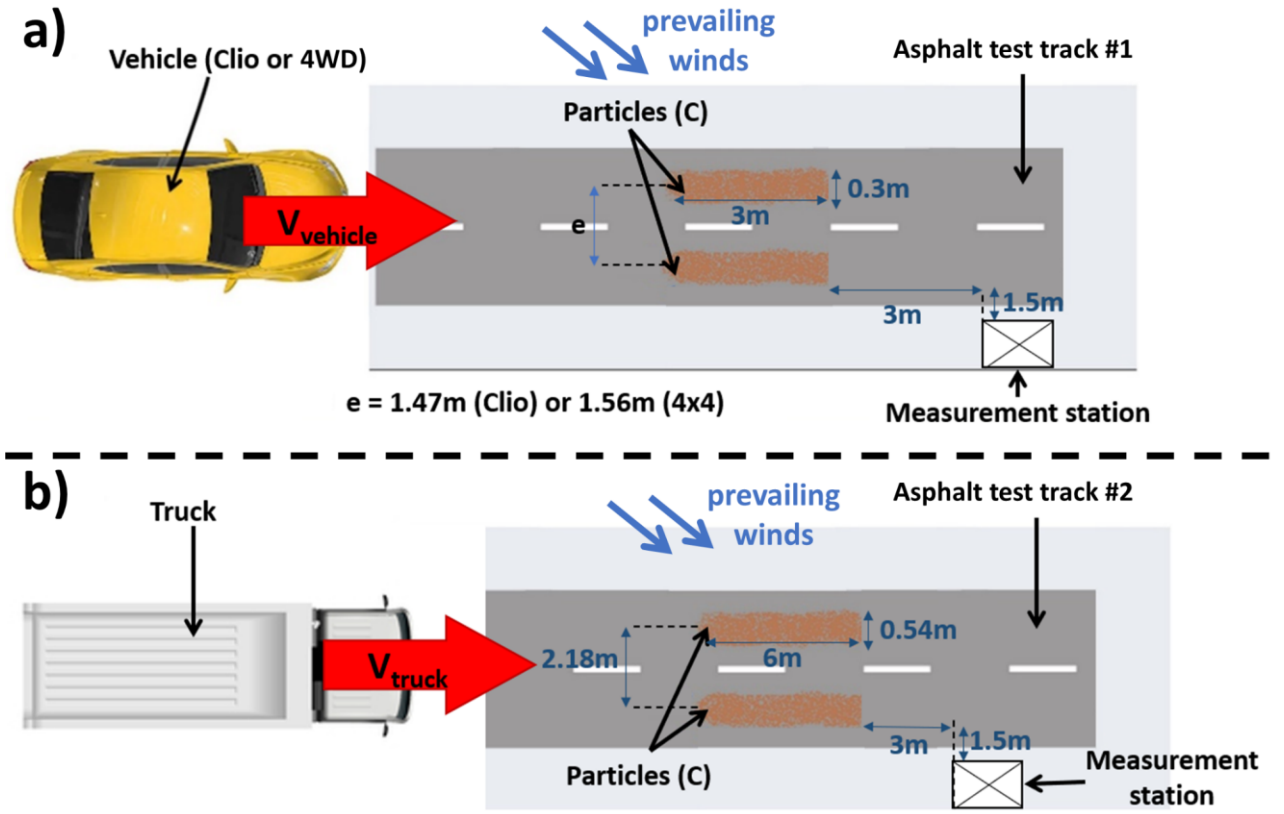

Figure 4: Diagram of the experimental setup on the track for a) Renault Clio III and 4WD Ford Ranger; b) Volvo FMX truck (diagram is not to scale)

A BIRAL SWS-100 visibility sensor is used to measure the reduction in visibility from the side of the road due to the passing test vehicles. The visibility measurements are carried out at the same place than the dust concentration ones to establish a direct relationship between both physical parameters. The meteorological optical sensor ranges from 0.01 to 2 km. This measurement range includes the road safety conditions. In France, for example, the maximum speed must be reduced to 50 km/h when the visibility on the road is less than 50 m. Prior to the testing, the visibility sensor has been calibrated using a Calibration Reference Plaque as recommended by the manufacturer (BIRAL, 2014). Figure 5 displays the diagram of the measurement station with the OPC, the visibility sensor and the weather station.

Six tests are carried out with the 4WD vehicle, ten with the Clio and twenty-two with the truck while varying the different parameters (vehicle speed, particle type and mass per unit area). Table 3 summarizes the main characteristics. For practical reasons of time and quantity of particles available, all the possible combinations of parameters could not be tested. The experimental design is based on the Tagushi method (Tagushi and Konishi, 1987), which makes it possible to highlight the impact of the experimental parameters on the final results with a limited number of trials. Because a considerable amount of effort has been already devoted to examine the effects of vehicle speed on dust emissions in the literature (Moosmüller et al., 2005; Gillies et al., 2005; Thenoux et al., 2007; Kuhns et al., 2010), the test plan has been primarily designed to focus on the effects of the "state of degradation of the road", which is characterized by the quantity of particles on the ground. Some configurations are tested several times to ensure the repeatability of the measurements by carrying out the same test twice in a row. Nine repeatability tests are thus carried out to assess uncertainties. Error bars are therefore presented with the results taking these uncertainties into account.

After each test, a sample of the particles remaining on the ground is taken for moisture content measurement (*M*, the ratio of the mass of water to the dry mass of the particles). For all the tests, $M = 2 \pm 0.7$ % (the particles absorbed some moisture during the experiments). The soils in hygroscopic equilibrium with the air between 50% and 85% of relative humidity have a gravimetric water content between 2 and 7 times higher than the present results (Ravi and D'Odorico, 2005). Relative humidity has no effect here because moisture exchanges between dry particles and atmosphere require hours or even days (Ravi et al., 2006). This effect, however, is not negligible, as shown by Muleski et al. (2005), according to which a soil with a water content changing from 4% to 8% decreases its PM_{10} emissions by 75%.

The test track here is cleaned up between two tests using a leaf blower. Furthermore, the track is also swept up manually to make sure that all remaining particles within the asphalt voids are removed.

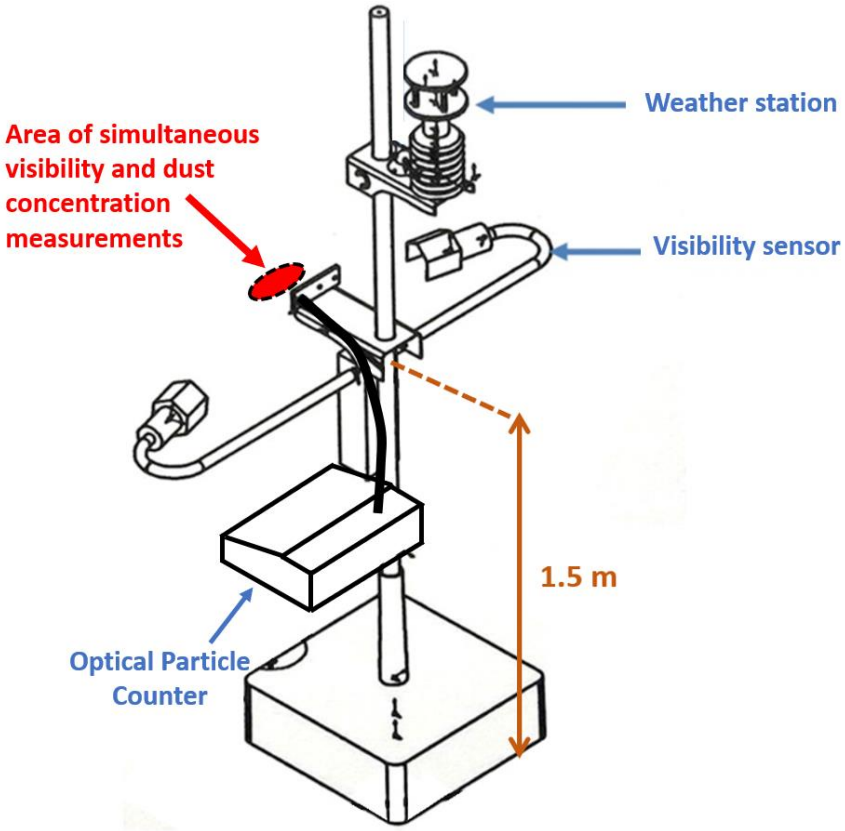

Figure 5: Diagram of the measurement station. Wind speed and direction, visibility reduction and dust concentration are measured simultaneously (Sediki et al., 2018)

Table 3: Test configurations

Vehicle	Particles*	Speed (km/h)	Concentration (g/m²)	Vehicle	Particles*	Speed (km/h)	Concentration (g/m²)
Clio III	SVE	30	200	Truck Volvo FMX	GC	30	200
			400				400
		45	200				600
			400			45	200
		60	200		SVE	30	200
			400				400
			600				600
4x4 Ford Ranger	SVE	60	200			45	200
			400				400
			600		SS	30	200
							400
							600
						45	200
							400
* GC: Green Clay SVE: Silt from Val d'Europe SS: Silt from Strasbourg SMD: Silt from Marche les Dames					SMD	30	200
							400
							600
						45	400

2.4 Data processing

2.4.1 Sampling efficiency of the optical particle counter

The OPC measures PM_{10} concentrations by aspiration of the atmospheric aerosol, which are then transported through a nozzle to the optical measurement volume. In this study, the sampling efficiency is not 100% because of the sub-isokinetic and anisoaxial conditions (non-alignment of wind and sampling directions) as well as some inertial transmission losses in the nozzle. The sensor measurement must therefore be corrected by taking the sampling efficiency η_{sample} into account. The sampling efficiency is defined as the product of the aspiration and the transport efficiencies (Willeke and Baron, 2001):

$$\eta_{sample} = \eta_{asp} \times \eta_{trans} \tag{3}$$

The aspiration efficiency η_{asp} is defined as the concentration of the particles entering the nozzle divided by their concentration in the ambient environment from which the sample is taken. The relationship developed by Hangal and Willeke (1990) thanks to quantifying experimentations is expressed as:

$$\eta_{asp} = 1 + \left[\left(\frac{U_0}{U}\right)cos\theta - 1\right]\frac{1 - \left[1 + \left[2 + 0.617\left(\frac{U}{U_0}\right)\right]S_{tk}{}'\right]^{-1}}{1 - [1 + 2.617S_{tk}{}']^{-1}}[1 - [1 + 0.55S_{tk}{}'\exp(0.25S_{tk}{}')]^{-1} \tag{4}$$

$$S_{tk}{}' = S_{tk}.\exp(0.022\theta) \tag{5}$$

for $0° \leq \theta \leq 60°$, where θ is the angle between the wind and the sampling directions, U_0 and U are the wind and the sampling velocities ($m.s^{-1}$), respectively, and S_{tk} is the Stokes number of the particle (Eq. (6)):

$$S_{tk} = \frac{1}{18}\frac{\rho_p d_p U_0}{\mu L_c} \tag{6}$$

where ρ_p is the particle density ($kg.m^{-3}$), d_p is the particle diameter (m), μ is the dynamic air viscosity ($18.5.10^{-6}$ $kg.m^{-1}.s^{-1}$ at 20°C) and L_c is a characteristic length (here the nozzle diameter, i.e., L_c=0.008 m).

They extended this relationship for $60° \leq \theta \leq 90°$ (Eq. (7)):

$$\eta_{asp} = 1 + \left[\left(\frac{U_0}{U}\right)cos\theta - 1\right]\left[3Stk^{\sqrt{\frac{U}{U_0}}}\right] \tag{7}$$

The transport efficiency η_{trans} is defined as the fraction of aspirated particles that are transported through the inlet to the measurement volume. This parameter depends on both the gravitational deposition and the inertial losses. To our knowledge, Okazaki et al. (1987) are the only authors who studied gravitational settling transport efficiency. They carried out testing using a 200-mm nozzle so, consequently, their results cannot be extended to the present tests, for which the length of the nozzle is 900 mm. However, the settling velocity of the particles (*≈0.008 $m.s^{-1}$*) is negligible compared to the aspiration velocity (*U=0.47 $m.s^{-1}$*). Hence, the gravitational deposition is not taken into account and only the inertial losses are considered. Inertial losses have been studied by Liu et al. (1989) who propose the following inertial transport efficiency relationship for sub-isokinetic sampling (Eq. (8)):

$$\eta_{trans} = \frac{1 + \left[\frac{U_0}{U} - 1\right] / \left[1 + \frac{2.66}{S_{tk}{}^{2/3}}\right]}{1 + \left[\frac{U_0}{U} - 1\right] / \left[1 + \frac{0.418}{S_{tk}}\right]} \tag{8}$$

Here, the concentrations measured by the OPC are corrected using Eq. (9):

$$C = \frac{C_{measured}}{\eta_{sample}} \tag{9}$$

2.4.2 Emission factor calculation

The present analysis focuses on PM_{10} emissions, which corresponds to the particles range generally studied in the literature focusing on the problem of dust emissions on unpaved roads (Etyemezian et al., 2003; Gillies et al., 2005; USEPA, 2006; Kuhns et al., 2010). We consider that the OPC measurements represent the PM_{10} concentration at a height corresponding to the vertical distance of the sensor from the ground (1.5 m). For each test, the time series of PM_{10} are examined regarding the peak of dust concentration induced by the vehicle. This peak value is defined by the measurements between the beginning of the concentration rise above the background level and the return to a background concentration defined as the average PM_{10} concentrations measured between two tests (i.e., 10 µg.m^{-3}). The emissions factor (*EF*) per vehicle pass is estimated using the sum of the PM_{10} concentrations measured per second, according to Eq. (10) (Gillies et al., 2005):

$$EF = \sum_{start\ time\ of\ peak}^{end\ time\ of\ peak} U_0 \times C \times \Delta z \times \Delta t \times 1000 \quad (10)$$

where *EF* is the estimated emission factor of PM_{10} in grams per vehicle kilometer traveled (gPM_{10}.vkt^{-1}), U_0 is the 30-seconds average wind speed (m.s^{-1}), *C* is the 1-s PM_{10} concentration (g.m^{-3}) measured by the OPC and corrected according to Eq. (9), Δz is the dust plume vertical interval represented by the OPC (taken as 1.5 m) and Δt is the time during which the plume impacts the OPC (s). A factor 1000 is required to obtain the final result in dust emission per kilometer.

The measurements are carried out on the side of the test track, where the dispersion area of the dust plume is not very large (within a few meters). It is therefore considered that the measurements from the single sensor are representative of the average particle concentration in the plume. The visual observations made throughout the tests confirm this assumption. Furthermore, on the roadside, the near-source redeposited dust particles are measured. These are not taken into account in the inventories for air quality modelling at regional-scale (Veranth et al., 2003) but they have to be considered in visibility reduction studies.

3. Results and discussion

3.1 Emission factors

Figure 6 presents the EFs for the tests with the Renault Clio and the 4WD vehicle. In Figure 6-a, the results are compared with those obtained by Gillies et al. (2005) with a Dodge Neon (weight: 1,176 kg), a Ford Taurus (weight: 1,516 kg) and a GMC G20 van (weight: 3,100 kg). It should be noted that the curves proposed by Gillies et al. (2005) were obtained with nine different vehicle speeds (16, 24, 32, 40, 48, 56, 64, 72 and 81 km.h^{-1}). They show that EFs are linearly correlated with the vehicle speed and that the slopes of the curves depend on the vehicle weight. According to these criteria, the expected EF results for the 4WD Ford Ranger (with a weight of 2,300 kg) should have been between the dotted line and the dashed line in Figure 6-a. However, they actually are between one and two orders of magnitude lower. This difference may be accounted for by the presence of mud flaps behind the tires of the 4WD vehicle, which may significantly reduce emissions. For confirmation, more tests need to be carried out with the same vehicle with and without mud flaps to improve our understanding of dust emission mitigation related to the presence of accessories on the wheels. This impact, notably obturating discs on the rims, has been studied by Gérardin (2009).

The Renault Clio used here is approximately the same weight as the Dodge Neon and generates comparable EF results for the lowest quantity of particles on the ground (200 g.m^{-2}) whatever the vehicle speed. Indeed, the average difference is only 17 g.vkt^{-1} between the "Dodge Neon" full black line and the blue dots in Figure 6-a. The test results with the Clio show that a doubling of the surface degradation from 200 to 400 g/m² increases EF sevenfold (on average). A tripling of the degradation from 200 to 600 g/m² generates an 18-fold increase in EF. These results demonstrate that it is crucial to take unpaved road surface condition into account in order to accurately quantify the unpaved road propensity for generating dust. To date, this problem has not been considered in the already available models developed to assess EFs. Figure 6-b shows that EF results using AP-42 models (Eq. (1) and (2)) are between 1,800 and 3,400 gPM_{10}.vkt^{-1}, which is more than one order of magnitude above the present experimental results. These models have been developed from tests on soils with low silt contents, while this content is significantly high in the particles used here (more than 95%). This may explain these large differences. It should also be noted that the USEPA model for public roads (Eq. (2)) does not take the vehicle mass into account and, therefore, gives the same dust emission estimate for both the 4WD vehicle and the Clio (solid green curve in Figure 6-b).

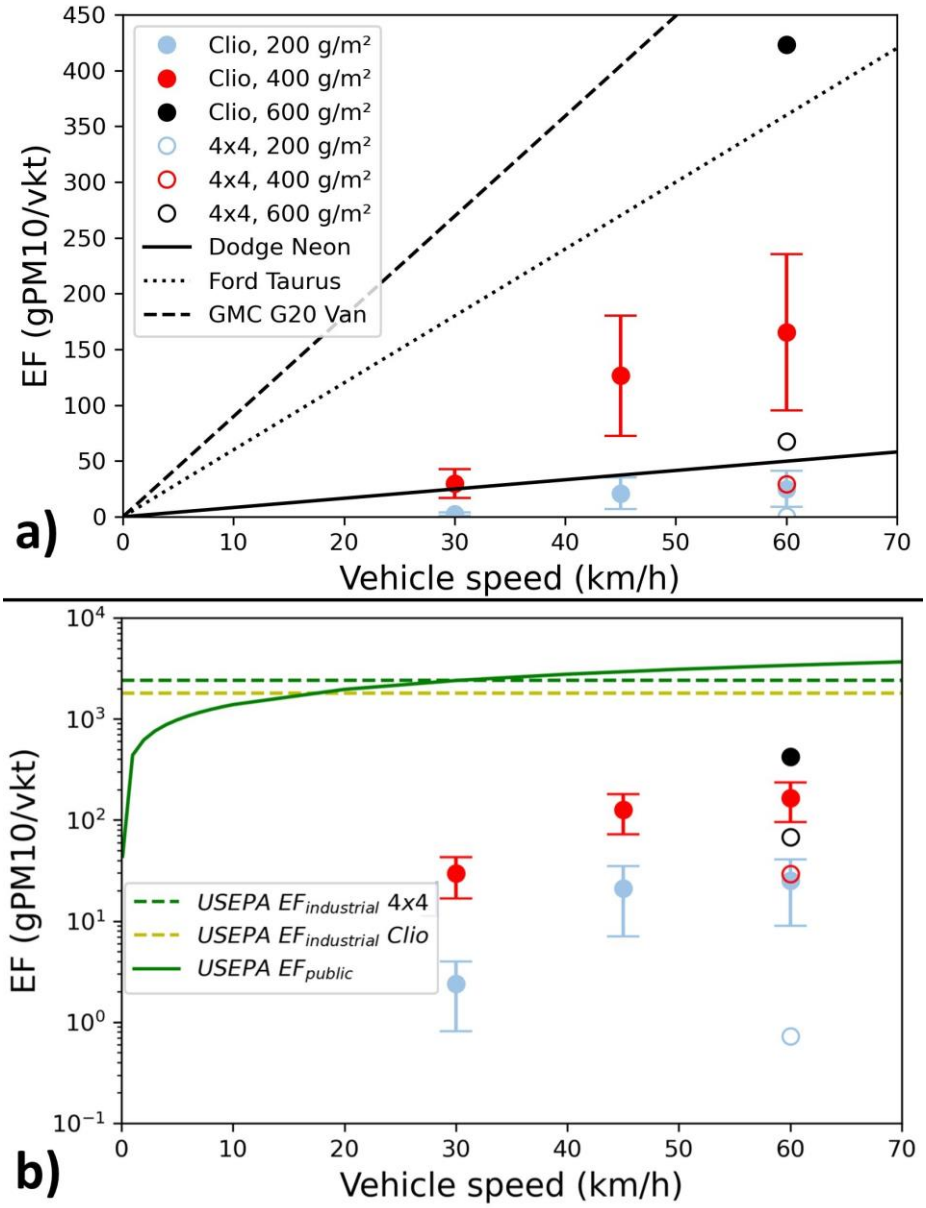

Figure 6: EFs as a function of vehicle speed and mass of particles per unit area for the tests with the Renault Clio and the 4WD Ford Ranger. a) Experimental data are compared with the results obtained by Gillies et al. (2005) with a Dodge Neon (solid line), a Ford Taurus (dotted line) and a GMC C20 Van (dashed line); b) Same results in a semi-log scale and comparison with the AP-42 models (Eq. (1): dotted lines, Eq. (2): solid line).

Figure 7 shows the EF values obtained for the tests with the Volvo truck. These results are compared with those obtained by Gillies et al. (2005) with an US Army M977 HEMTT cargo truck. This vehicle has the same number of wheels but is only half the weight of the Volvo truck (17,727 kg against 32,000 kg). To the authors' knowledge, no data on dust EFs for trucks with the same weight as the Volvo truck used in the present study is currently available in the literature. The results are also compared with USEPA modeling results for public roads (Eq. (2)). Modeling results for industrial roads (Eq. (1)) are not displayed in the figures because EF values are too high (about 8,000 $gPM_{10}.vkt^{-1}$, regardless of the truck speed).

In the present study, all the particles tested have approximately the same silt content (between 95 and 100%). The USEPA model (green curves in Figure 7) gives similar EFs for all of them. However, there are some significant differences between the results of this study depending on the type of particles. These significant discrepancies prove that the silt content is not sufficient to assess the propensity of a soil to generate dust. As for the Clio and the 4WD vehicle, the results with the truck show that the state of degradation of the soil (mass of particles per unit area above the ground) has a strong impact on the emissions of dust.

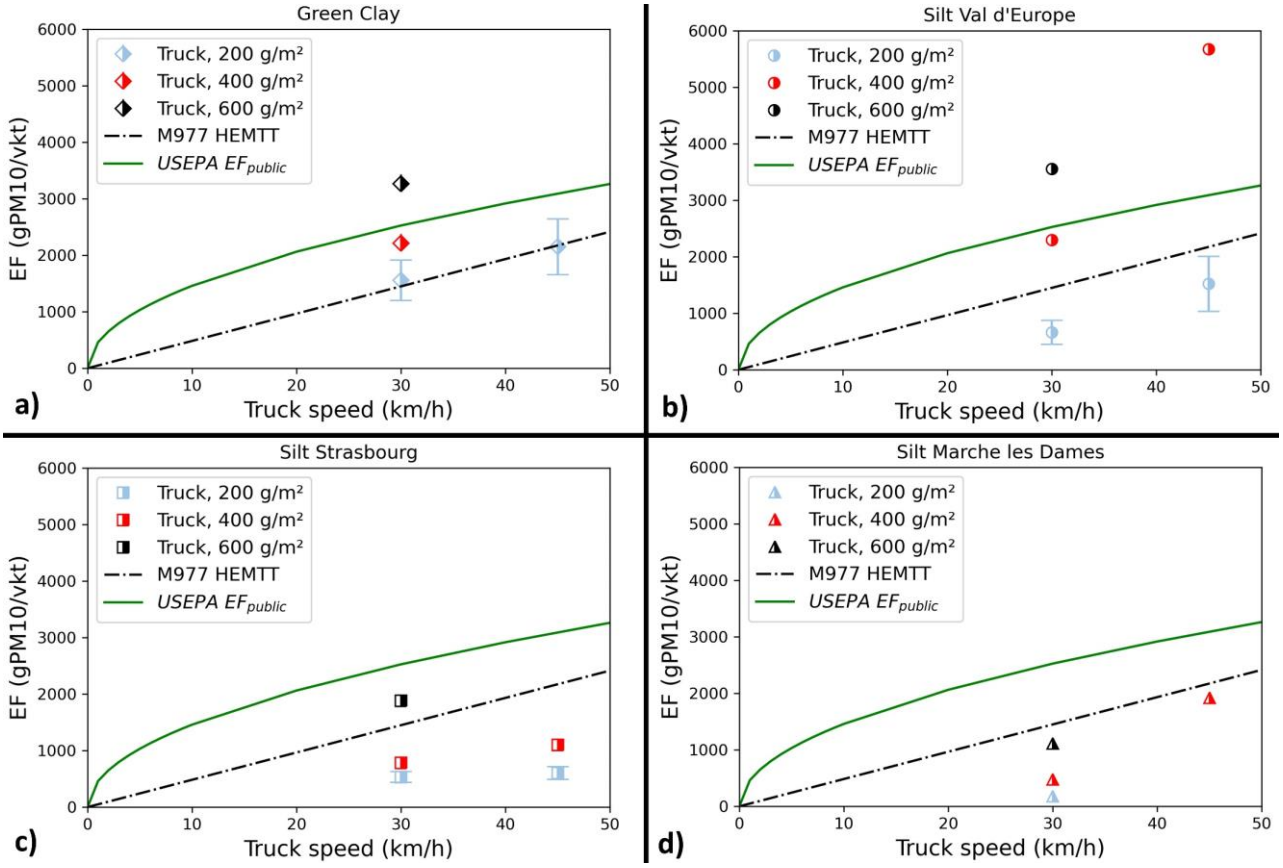

Figure 7: EFs as a function of vehicle speed and mass of particle per unit area for the tests with the truck Volvo FMX on a) green clay, b) silt from Val d'Europe, c) silt from Strasbourg and d) silt from Marche les Dames. Experimental data are compared with the results obtained by Gillies et al. (2005) with a M977 HEMTT truck (broken line) and using the AP-42 model for public roads (Eq. (2), green line).

Based on these experimental results and observations, a model for the quantification of EFs is developed. The first step consists in identifying the most relevant parameters. It is well established in the literature (Gillies et al., 2005; Kuhns et al., 2010) that the EF is linearly proportional to the vehicle momentum. The experimental data discussed here also show that the soil degradation state is a parameter of paramount importance. Furthermore, the type of particles must be taken into account. Regarding the test data obtained with the truck, the silt content is not a relevant parameter contrary to the clay content (%<2µm), which allows to distinguish between the four types of particles. Finally, the tests carried out with the 4WD vehicle show that the impact of mud flaps behind the tires is also significant. These appendices are considered through a weighting factor. With a form similar to the USEPA models (Eq. (1) and (2)), the following equation is proposed (Eq. (11)):

$$EF_{model} = \alpha \times M_{om} \times \left(\frac{c}{c_{ref}}\right)^{\beta} \times \left(\frac{D}{D_{ref}}\right)^{\gamma} \times f_{mf} \quad (11)$$

where EF_{model} is expressed in kg.m^{-1} to homogenize the units in the equation (to be multiplied by 10^6 to be expressed in g.vkt^{-1}), M_{om} is the vehicle momentum (M_{om}=S.W, in kg.m.s^{-1}), c is the clay content (%<2µm) of the particles, c_{ref} is a reference clay content (arbitrarily chosen at 12 %, which corresponds to the minimum value of the particles used in this study), D is the soil surface degradation (mass of particles per unit area above the ground in kg.m^{-2}), D_{ref} is a degradation reference (arbitrarily chosen at 0.2 kg.m^{-2}, the minimum value studied here) and f_{mf} is a weighting factor taking the influence of mud flaps into account. α, β and γ are empirical parameters.

Performing a multiple regression on the experimental data obtained with the Clio and the truck and considering a 95% confidence interval, the parameters α, β and γ of the model can be established. The parameter f_{mf} is determined by fitting the data obtained with the 4WD vehicle with the previously established model. The final model is given by Eq. (12):

$$EF_{model} = 7.6 \times 10^{-10} \times M_{om} \times \left(\frac{c}{12}\right)^{1.05} \times \left(\frac{D}{0.2}\right)^{1.71} \times f_{mf} \quad with \begin{cases} f_{mf} = 1 \; if \; no \; mud \; flaps \\ f_{mf} = 0.15 \; if \; mud \; flaps \end{cases} \quad (12)$$

This model shows that the surface degradation state is the parameter that most affects EF. The presence of mud flaps behind the tires decreases EFs by a factor of 7. Additional tests need to be carried out to validate this observation and generalize this result. It is also important to note that this model is developed using soils with high silt contents. Further

research with sandy soils is necessary to extent the application of the model to a wider range of soils. A robust model should be able to account for both clay and silt contents.

Figure 8 presents the comparison between the EF values determined experimentally and those modeled using Eq. (12). There is a good correlation between the theoretical and experimental data, up to an EF value of 3000 $gPM_{10}.vkt^{-1}$. Beyond this limit, the model becomes a less reliable tool to quantify the emissions, the differences between prediction and measurements reaching a factor of 2. However, these values correspond to very high dust emissions caused by the trucks which are not realistic on construction sites. Indeed, water is sprayed on the traffic lanes well before such emission levels are reached because of the very significant reductions in visibility such dust plumes would imply.

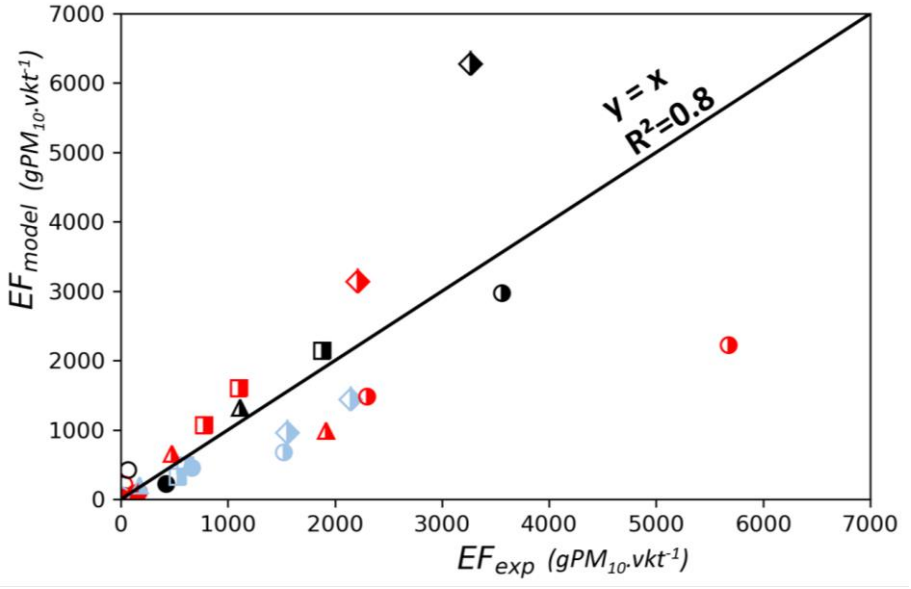

Figure 8: Comparison between the model of Eq. (12) and the experimental data. Symbols are the same as in Figures 6 and 7.

3.2 Visibility reduction

Many studies have established a relationship between PM_{10} mass concentration and visibility reduction (D'Almeida, 1986; Dayan et al., 2008; Jugder et al., 2014; Baddock et al., 2014; Camino et al., 2015). Table 4 summarizes the available models, where V is the visibility in km and $\overline{PM_{10}}$ the average mass concentration of particles below 10 µm (in $\mu g.m^{-3}$).

Table 4: Empirical model equations relating PM_{10} mean concentration (in $\mu g/m^3$) to visibility (V in km)

Authors	Empirical equation	Measurement location
D'Almeida (1986)	$\overline{PM_{10}} = 914 \times V^{-0.73} + 19$	Visibility and PM10 concentration measurements carried out in Agadez (Niger). Source of dust emissions (desert) located several hundreds of km from the measurement sites.
Dayan et al. (2008)	$\overline{PM_{10}} = -505.\ln(V) + 2264$	PM10 concentration measurements carried out in the Negev desert. Visibility measurement at Hazerim airport (Israel) located 50 km away.
Jugder et al. (2014)	$\overline{PM_{10}} = 486 \times V^{-0.78}$	Visibility and PM10 measurements carried out at Zamyn-Uud in the Gobi Desert, near the dust emission source.
Baddock et al. (2014)	$\overline{PM_{10}} = 556 \times V^{-1.03}$	PM10 concentration measurement carried out in Buronga (Australia). Visibility measurements in the next town (Mildura) located 12 km away. Sources of dust emission are located between 10 and 100 km from these stations.
Camino et al. (2015)	$\overline{PM_{10}} = 1772 \times V^{-1.10}$	Visibility and PM10 concentration measurements carried out in Izaña (Spain). Source of dust emissions (desert) located at several hundred km from the measurements.

The main sources of dust emissions in these studies come from deserts. It is also recognized that PM_{10} concentration is a good indicator of how visibility on gravel roads can be reduced (Edvarsson and Magnusson, 2009). Figure 9 presents the comparison between the models described in Table 4 and the experimental measurements obtained during the present study. Regarding the test results, PM_{10} concentration corresponds to the average value measured between the beginning and the end of the peak of dust concentration generated by the passage of the test vehicle (Eq. (13)). The visibility is averaged over the same period of time.

$$\overline{PM_{10}} = \frac{1}{N} \sum_{start\ time\ of\ peak}^{end\ time\ of\ peak} C \tag{13}$$

where C is the 1-s PM_{10} concentration ($\mu g.m^{-3}$) measured by the OPC and corrected according to Eq. (9), and N is the number of concentration values measured during the period for which the dust plume impacts the OPC.

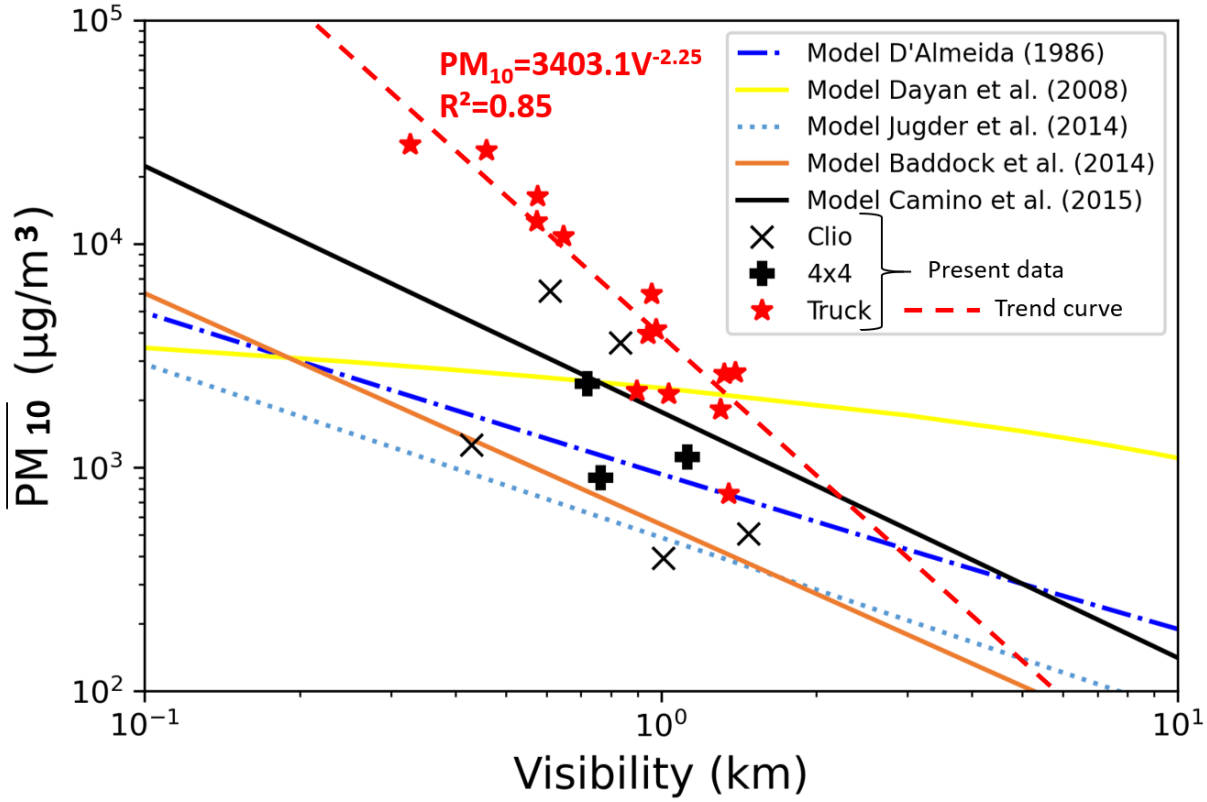

Figure 9: Relationship between the average visibility and the average PM10 concentration on the roadside. The experimental data are compared with the model results of D'Almeida (1986), Dayan et al. (2008), Jugder et al. (2014), Baddock et al. (2014) and Camino et al. (2015). These models are detailed in Table 4.

For the same level of PM_{10}, the Renault Clio and the 4WD vehicle reduce visibility more significantly than the truck. Indeed, the truck emits coarser particles which have a lower mass scattering efficiency compared to the small particles (Moosmüller et al., 2005). Then, PM_{10} concentration is not the best indicator of visibility reduction caused by light vehicles (Clio and 4WD Ford Ranger), as shown by the scattered corresponding experimental data. On the other hand, regarding the experimental data obtained with the truck, the following power law provides a relatively accurate estimate (R^2=0.85):

$$\overline{PM_{10}} = 3403.V^{-2.25} \tag{14}$$

By comparing this model with the models of the literature (Figure 9), a steeper slope is observed. This can be accounted for by the fact that the present model has been developed using simultaneous dust and visibility measurements carried out at the same location point, which is not the case for the other models. They, indeed, were developed to address this issue at a regional scale. The model developed here should therefore be more relevant regarding the consideration of visibility reduction on construction sites, keeping in mind that reduced visibility is mainly localized on the traffic lanes where trucks are circulating.

4 Conclusions

In this study, the dust emissions generated by the traffic of a passenger car, a 4WD vehicle and a truck are examined. In order to simulate the traffic of vehicles on unpaved roads, four types of particles (green clay, silt from Val d'Europe, silt from Strasbourg and silt from Marche les Dames) are spread on a test track at different mass per unit area (200 g/m², 400 g/m² and 600 g/m²). This simulates various states of road surface degradation. Vehicles are driven over the particle beds at different speeds (30, 45 and 60 km/h) and the concentrations of suspended dust emitted and the visibility reduction are measured from the roadside.

The main findings of this study are:

- The state of soil surface degradation appears to have a key influence on dust emission factors. A doubling of the mass of particles per unit area above the ground generates three times more dust emissions from the vehicles. However, this is not taken into account in classical models for emission factors estimation;

- Silt content (% < 75 µm) should not be the single parameter considered to assess particle lift. For fine soils, the percentage of clay particles (%< 2 µm) is particularly relevant to quantify the soil propensity for emitting dust;

- The vehicle momentum is not a sufficient criterion to characterize dust emission potential. The impact of appendices like mud flaps behind the tires could significantly reduce vehicle emissions by a factor of 7. The aerodynamic drag of the vehicles may also play a key role. More work needs to be carried out to understand this effect through testing with vehicles having the same momentum but very different geometry;

- The visibility reduction caused by PM_{10} emissions from truck traffic can be accurately modeled using a power law. This, however, is not the case for lighter vehicles because they raise finer particles with a higher mass scattering efficiency.

Finally, the established emission factor is a first step toward the consideration of the progressive increase in dust emissions due to the evolution of surface degradation under vehicle traffic. Future experimental campaigns need to be carried out on unpaved roads to compare actual emissions with those experimentally obtained in this study with particles spread on an asphalt test track. The present results highlight the crucial need to take the degradation state of the road into account when modeling dust emissions. This parameter should be further studied in order to establish a robust equation that could be implemented in atmospheric dispersion models. When used with the visibility reduction model, it would then be possible to consider safety risks on construction sites and anticipate the watering of traffic lanes. These results are part of an approach to optimise the use of water on earthmoving sites. When some water is sprayed on the soil, the particles on the surface form a crust that limits dust emissions. This phenomenon could be examined in future works by spraying liquid soil suspensions on the road before driving the vehicles. Moreover, the dust mitigation effect of mud flaps is of particular interest and could be the subject of further research work. Wind tunnel testing could be carried out to examine how such appendices affect the airflow in the wake of vehicles.

CRediT authorship contribution statement

Mickael Le Vern: Conceptualization, Data curation, Investigation, Methodology, Resources, Validation, Writing – original draft, Writing – review & editing. **Andry Razakamanantsoa:** Conceptualization, Funding acquisition, Methodology, Resources, Supervision, Validation, Writing – review & editing. **Frédéric Murzyn:** Conceptualization, Methodology, Supervision, Validation, Writing – review & editing. **Frédérique Larrarte:** Conceptualization, Methodology, Supervision, Validation, Writing – review & editing. **Véronique Cerezo:** Methodology, Resources, Validation, Writing – review & editing.

Acknowledgements

The authors would like to express their gratitude to the Fédération Nationale des Travaux Publics (grant number RP2_E18101) and the Région Pays de la Loire (grant number GHPAI3) for their financial support. Special thanks to Ouardia Sediki, Erwann Rayssac, Sébastien Buisson and Daniel Bodenes for their contribution during the tests and to Marie-Bertille Couëdel who checked the English editing. Sincere thanks also to Pascal Insenga (Vinci Construction Terrassement), Laurent Desmurs (Bouygues Travaux Publics), Benjamin Daubilly (UMTM, Union des Métiers de la Terre et de la Mer) and Philippe Gotteland (FNTP, Fédération Nationale des Travaux Publics) for the technical contribution, the supervision and the link with the profession.

Conflicts of Interest

The authors declare no conflict of interest.

References

Ashley, W.S., Strader, S., Dziubla, D.C., Haberlie, A. (2015) Driving blind: Weather-related vision hazard and fatal motor vehicle crashes. *Bulletin of the American Meteorological Society* **96**:755-779, doi:10.1175/BAMS-D-14-00026.1

ASTM (2017) ASTM D2487-17e1, Standard practice for classification of soils for engineering purposes (Unified Soil Classification System), *ASTM International, West Conshohocken, PA*

ASTM (2019) ASTM C837-09, Standard test method for methylene blue index of clay, *ASTM International, West Conshohocken, PA*

Baddock, M.C., Strong, C.L., Leys, J.F., Heidenreich, S.K., Tews, E.K., McTainsh, G.H. (2014) A visibility and total suspended dust relationship. *Atmospheric Environment* **89**:329-336, doi:10.1016/j.atmosenv.2014.02.038

Bhattachan, A., Okin, G.S., Zhang, J., Vimal, S., Lettenmaier, D.P. (2019) Characterising the role of wind and dust in traffic accidents in California. *GeoHealth* **3**(10):328-336, doi:10.1029/2019GH000212

BIRAL (2014) Operation and maintenance manual - SWS Present Weather Sensors. *Technical Manual, Bristol Instrumental and Research Associates Limited*

Camino, C., Cuevas, E., Basart, S., Alonso-Pérez, S., Baldasano, J.M., Terradellas, E., Marticorena, B., Rodriguez, S., Berjon, A. (2015) An empirical equation to estimate mineral dust concentrations from visibility observations in Northern Africa. *Aeolian Research* **16**:55-68, doi:10.1016/j.aeolia.2014.11.002

D'Almeida, G.A. (1986) A model for Saharan dust transport. *Journal of Applied Meteorology and Climatology* **25**(7):903–916, doi: 10.1175/1520-0450(1986)025<0903:AMFSDT>2.0.CO;2

Dayan, U., Ziv, B., Shoob, T., Enzel, Y. (2008) Suspended dust over southeastern Mediterranean and its relation to atmospheric circulations. *International Journal of Climatology* **28**(7):915–924, doi: 10.1002/joc.1587

Edvarsson, K., Magnusson, R. (2009) Monitoring of dust emission on gravel roads: Development of a mobile methodology and examination of horizontal diffusion. *Atmospheric Environment* **43**:889-896, doi: 10.1016/j.atmosenv.2008.10.052

Etyemezian, V., Kuhns, H., Gillies, J., Green, M., Pitchford, M., Watson, J. (2003) Vehicle-based road dust emission measurement: I—methods and calibration. *Atmospheric Environment* **37**(32):4559-4571, doi: 10.1016/S1352-2310(03)00528-4

Faber, P., Drewnick, F., Borrmann, S. (2015) Aerosol particle and trace gas emissions from earthworks, road construction and asphalt paving in Germany: Emission factors and influence on local air quality. *Atmospheric Environment* **122**:662-671, doi: 10.1016/j.atmosenv.2015.10.036

Flores-Márgez, J.P., Shukla, M.K., Deb, S. (2014) Mapping of airborne particulate matter collected using two sensors along US-Mexico border. *Journal of Environmental & Analytical Toxicology* **4**(2):1-10, doi: 10.4172/2161-0525.1000206

Gérardin, F. (2009) Étude expérimentale et numérique de la dispersion d'aérosols dans le sillage d'une roue de véhicule. *PhD Thesis, Université de Lorraine, 238 p. (in French).*

Gérardin, F., Midoux, N. (2015) Attenuation of road dust emissions caused by industrial vehicle traffic. *Atmospheric Environment* **127**:46-54, doi: 10.1016/j.atmosenv.2015.12.006

Gillies, J.A., Etyemezian, V., Kuhns, H., Nikolic, D., Gillette, D.A. (2005) Effect of vehicle characteristics on unpaved road dust emissions. *Atmospheric Environment* **39**(13):2341-2347, doi: 10.1016/j.atmosenv.2004.05.064

GTR (2000) *Guide français pour la Réalisation des remblais et des couches de forme*. IFSTTAR-CEREMA, Ministère de l'Écologie, du Développement durable et de l'Aménagement du territoire, 2eme édition (in French)

Hangal, S., Willeke, K. (1990) Overall efficiency of tubular inlets sampling at 0-90 degrees from horizontal aerosol flows. *Atmospheric Environment* **24**(9):2379-2386, doi: 10.1016/0960-1686(90)90330-P

Hichri, Y., Descartes, S., Cerezo, V., Do. M.-T. (2019). Understanding the behavior of fine particles at the tire/road interface. *Tribology Internationnal* **149**, 105635, doi: 10.1016/j.triboint.2019.02.043

Hussein, T., Johansson, C., Karlsson, H., Hansson, H.-C. (2008). Factors affecting non-tailpipe aerosol particle emissions from paved roads: On road measurements in Stockholm, Sweden. *Atmospheric Environment* **42**(4):688-702, doi: 10.1016/j.atmosenv.2007.09.064.

ISO (2014). ISO 17892-1/2014 – Laboratory testing of soil – Part 1: Determination of water content. *International Organization of Standardization, Geneva, Switzerland*

ISO (2018). ISO 17892-12/2018 – Laboratory testing of soil – Part 12: Determination of liquid and plastic limits. *International Organization of Standardization, Geneva, Switzerland*

Jugder, D., Shinoda, M., Kimura, R., Batbold, A., Amarjargal, D. (2014) Quantitative analysis on windblown dust concentrations of PM_{10} ($PM_{2.5}$) during dust events in Mongolia. *Aeolian Research*, **14**:3-13, doi: 10.1016/j.aeolia.2014.04.005

Kuhns, H., Knipping, E.M., Vukovich, J.M. (2005) Development of a United States-Mexico emission inventory for the big bend regional aerosol and visibility observational (BRAVO) study. *Journal of the Air & Waste Management Association* **55**(5) :677-692, doi : 10.1080/10473289.2005.10464648

Kuhns, H.D., Gillies, J., Etyemezian, V., Nikolich, G., King, J., Zhu, D., Uppapalli, S., Engelbrecht, J., Kohl, S. (2010) Effect of Soil Type and Momentum on Unpaved Road Particulate Matter Emissions from Wheeled and Tracked Vehicles. *Aerosol Science and Technology* **44**(3):187-196, doi:10.1080/02786820903516844

Lankarani, K.B., Heydari, S.T., Aghabeigi, M.R., Moafian, G., Hoseinzadeh, A., Vossoughi, M. (2014) The impact of environmental factors on traffic accidents in Iran. *Journal of Injury & Violence Reearch* **6**(2):64-71, doi:10.5249/jivr.v6i2.318

Le Vern, M., Sediki, O., Razakamanantsoa, A.R., Murzyn, F., Larrarte, F. (2020a) Experimental assessment of dust emissions on compacted soils degraded by traffic. *Atmosphere* **11**, 369, doi:10.3390/atmos11040369

Le Vern, M., Sediki, O., Razakamanantsoa, A.R., Murzyn, F., Larrarte, F. (2020b) Experimental study of particle lift initiation on roller compacted sand-clay mixtures. *Environmental Geotechnics* doi:10.1680/jenge.19.00172

Le Vern, M., Razakamanantsoa, A.R., Murzyn, F., Larrarte, F., Cerezo, V. (2021) Study on a test track of dust resuspension induced by a vehicle. *In Proceedings of the 24th Transport and Air Pollution Conference, Graz, Austria, 30 March – 01 April 2021*

Liu, B.Y.H., Zhang, Z.Q., Kuehn, T.H. (1989) A numerical study of inertial errors in anisokinetic sampling. *Journal of Aerosol Science* **20**(3):367-380, doi: 10.1016/0021-8502(89)90012-8

Mie, G. (1908) Beiträge zur Optik trüber Medien, speziell kolloidaler Metallösungen, *Annalen der Physik* **330**(3):377-445, doi: 10.1002/andp.19083300302 (in German)

Moosmüller, H., Varma, R., Arnott, W.P., Kuhns, H.D., Etyemezian, V., Gillies, J.A. (2005) Scattering cross-section emission factors for visibility and radiative transfer applications: Military vehicles traveling on unpaved roads. *Journal of the air & Waste Management Association* **55**(11):1743-1750, doi: 10.1080/10473289.2005.10464763

Muleski, G.E., Cowherd, C., Kinsey, J.S. (2005) Particulate emissions from construction activities. *Journal of Air & Waste Management Association* **55**(6):772-783, doi:10.1080/10473289.2005.10464669

NIOSH (2012) Dust control Handbook for industrial minerals mining and processing. *Technical Report, Department of Health and Human Services, National Institute of Occupational Safety and Health, USA*

Noh, H., Lee, S., Yu, J. (2018) Identifying effective fugitive dust control measures for construction projects in Korea. *Sustainability 2018, 10, 1206;* doi: 10.3390/su10041206

Okazaki, K., Wiener, R.W., Willeke, K. (1987) The combined effect of aspiration and transmission on aerosol sampling accuracy for horizontal isoaxial sampling. *Atmospheric Environment* **21**(5):1181-1185, doi: 10.1016/0004-6981(87)90245-9

Pinnick, R.G., Fernandez, G., Hinds, B.D., Bruce, C.W., Schaefer, R.W., Pendleton, J.D. (1985) Dust generated by vehicular traffic on unpaved roadways: sizes and infrared extinction characteristics. *Aerosol Science and Technology*, **4**(1):99-121, doi: 10.1080/02786828508959042

Pope, C.A., Dockery, D.W. (2006) Health effects of fine particulate air pollution: Lines that connect. *Journal of the Air & Waste Management Association* **56**(6):709-742, doi:10.1080/10473289.2006.10464485

Ravi, S., D'Odorico, P. (2005) A field scale analysis of the dependence of wind erosion threshold velocity on air humidity. *Geophysical Research Letters* **32**(21), L21404, doi: 10.1029/2005GL023675

Ravi, S., Zobeck, T.M., Over, T.M., Okin, G.S., D'Odorico, P. (2006) On the effect of moisture bonding forces in air-dry soils on threshold friction velocity of wind erosion. *Sedimentology* **53**:597–609, doi: 10.1111/j.1365-3091.2006.00775.x

Sediki, O., Razakamanantsoa, A.R., Rayssac, E., Bodenès, D. (2018) Procédé et dispositif de détermination du coefficient et du potentiel d'émission de particules d'un matériau, et procédé de gestion d'une voie de circulation. *French patent N°1855260* (in French)

Serpell, A., Kort, J., Vera, S. (2013) Awareness, actions, drivers and barriers of sustainable construction in Chile. *Technological and Economic Development of Economy* **19**(2):272-288, doi:10.3846/20294913.2013.798597

571 Tagushi, G., Konishi, S. (1987) *Tagushi methods. Orthogonal arrays and linear graphs. Tools for quality engineering.*
572 American Supplier Institute Inc., MI.

573 Thenoux, G., Bellolio, J.P., Halles, F. (2007) Development of a methodology for measurement of vehicle dust generation
574 on unpaved roads. *Transportation Research Record: Journal of Transportation Research Board* 299-304, doi:
575 10.3141/1989-35

576 USEPA (1988) Control of Open Fugitive Dust Sources. *Report, Office of Air Quality Planning and Standards, Research*
577 *Triangle Park, Washington, USA*

578 USEPA (2006) Compilation of Air Pollutant Emission Factors, AP-42, Fifth Edition, Volume I, Chapter 13:
579 Miscellaneous Sources, 13.2.2 Unpaved Roads. *Office of Air Quality Planning and Standards, Research Triangle Park*.
580 (https://www.epa.gov/sites/production/files/2020-10/documents/13.2.2_unpaved_roads.pdf)

581 Vardaka, E., Cook, C.M., Lanaras, T., Sgardelis, S.P., Pantis, J.D. (1995) Effect of dust from a limestone quarry on the
582 photosynthesis of Quercus coccifera, and evergreen sclerophyllous shrub. *Bulletin of Environmental Contamination and*
583 *Toxicology* **54**(3):414-419, doi:10.1007/bf00195114

584 Veranth, J.M., Pardyjak, E.R., Seshadri, G. (2003) Vehicle-generated fugitive dust transport: analytic models and field
585 study. *Atmospheric Environment* **37**:2295-2303, doi:10.1016/S1352-2310(03)00086-4

586 Willeke, K., Baron, P.A. (2001) *Aerosol Measurement: Principles, Techniques, and Applications*. John Wiley & Sons
587 Inc., Hoboken, NJ, USA, doi:10.1002/9781118001684.

588 Williams, D.S., Shukla, M.K., Ross, J. (2008) Particulate matter emission by a vehicle running on unpaved road.
589 *Atmospheric Environment* **42**(16):3899-3905, doi: 10.1016/j.atmosenv.2008.02.003

590 Whitehouse, D. (2012) *Surfaces and their Measurement.* Boston: Butterworth-Heinemann. ISBN 978-0080972015

591